J. Cent. South Univ. (2020) 27: 1306−1319
DOI: https://doi.org/10.1007/s11771-020-4368-0

Springer

Seismic response of tunnel under normal fault slips by shaking table test technique

FAN Ling(樊玲), CHEN Jie-ling(陈捷翎), PENG Shu-quan(彭述权),
QI Bin-xi(祁彬溪), ZHOU Qi-wen(周启文), WANG Fan(王凡)

School of Resource and Safety Engineering, Central South University, Changsha 410083, China

Abstract: Mountain tunnel crossing a normal fault in seismically active zone is easily affected by normal fault slip and earthquake. It is necessary to study tunnel dynamic response under action of normal fault slip and earthquake. In this paper, a three-dimensional normal fault sliding device was designed, and a shaking table test was carried out to study tunnel seismic performance under normal fault slip. The results show that peak acceleration of lining is dominated by an existence of fault and direction of seismic excitation, not normal fault slip. And the incremental strains of lining in critical zone with 1.7 times fault thickness and centered in faults induced by normal fault slip and seismic excitation are larger than ones only by seismic excitation. And the incremental strains in critical zone increase with the increase of normal fault slip magnitude ranging from 0 to 2 mm. And normal fault slip results in a significant reduction of overall tunnel stiffness subjected to an earthquake. These experimental results provide a scientific reference for prevention and control measurement of tunnel damage under earthquake and normal fault slip.

Key words: tunnel; normal fault; earthquake; fault slip; shaking table test; peak acceleration

Cite this article as: FAN Ling, CHEN Jie-ling, PENG Shu-quan, QI Bin-xi, ZHOU Qi-wen, WANG Fan. Seismic response of tunnel under normal fault slips by shaking table test technique [J]. Journal of Central South University, 2020, 27(4): 1306−1319. DOI: https://doi.org/10.1007/s11771-020-4368-0.

1 Introduction

East African Great Rift Valley is seismically active zone, with many slipping normal faults, as well as Qinghai-Tibet Plateau [1, 2]. Most of railway tunnels and road tunnels constructed in these areas, such as Nahma railway project and Sichuan-Tibet railway, are lifelines engineering. And these tunnels cannot avoid fault and will be subject to earthquake activity with a high probability. The earthquake damage of tunnel will bring great trouble to the rescue work of these areas. In recent years, some surveys of earthquake damage of building show that the tunnel near or crossing fault zone is more easily damaged in seismically active zones such as Wenchuan, Chi-chi, Kobe [3−6]. The normal fault slipping is caused by tectonic stress or earthquake and results in permanent fault dislocation. This may induce tunnel failure or intensify the seismic damage of tunnel.

For crossing fault tunnel, tunnel elevation successive severe damage located in faulting zone happens when normal fault slips, and segmental tunnel maybe more easily dissipates normal fault slip effect than continuous one [7−9].

The failure mode of tunnel changes from bending and shearing failure to bending failure with normal fault dip increasing from 40° to 75° [10−12]. And the seismic response of tunnel critical zone

Foundation item: Project(51674287) supported by the National Natural Science Foundation of China
Received date: 2019-12-30; **Accepted date:** 2020-03-24
Corresponding author: PENG Shu-quan, PhD, Associate Professor; Tel: +86-13007499089; E-mail: pqr97linger@csu.edu.cn; ORCID: 0000-0002-6702-1004

with dual fault thickness and centered in tunnel fault is larger than those of other tunnel zones under seismic excitation, and the inverting and crowning of critical zone are severe damaged in shaking table test [13−20]. In the shaking table experiment, a roller device is set on the bottom of hanging wall to reduce the friction between rock strata and baseplate of model box. This device can be benefit to fault horizontal slip [13−15], but cannot simulate the permanent slipping of normal fault. In summary, tunnel seismic response under action of normal fault slip has not been reported in the above studies.

In this paper, three-dimensional normal fault permanent sliding device would be designed, and a shaking table test of tunnel model crossing normal fault under fault slip would be finished. And the seismic response of tunnel crossing normal fault under fault slip and seismic excitation would also be highlighted. This study provides a reference for prevention and control measures of tunnel seismic damage.

2 Shaking table test design

2.1 Engineering prototype

No. 3 tunnel of Kenya Nahma railway passes through a series of thick active faults in the east wing area of East African Great Rift Valley which is an active rift valley, expanding at a rate of 0.2−2 mm/year with frequent seismic activities [21, 22]. Thus, this tunnel is easily damaged by normal fault slip and earthquake action. This tunnel has a horseshoe-shaped section with a 400 mm thick lining made of C30 concrete. And the tunnel in fault is buried at depth of 46 m, and has a surrounding rock that is strongly weathered and weakly weathered trachyte. And this tunnel perpendicularly crosses an active fault that has a dip angle of nearly 90° and a thickness of 5−9 m.

2.2 Experimental equipment

A multi-functional shaking table test system of high-speed railway of Central South University was adopted in test. This system had a table size of 4 m× 4 m, a maximum load of 30 t, a maximum displacement in *X*, *Y* and *Z* directions of 250 mm, 250 and 160 mm, respectively, a maximum acceleration of 1.0*g*, and a working frequency ranging from 0.1 to 50 Hz. *X* direction was along tunnel axis direction; *Y* direction was horizontally perpendicular to tunnel axis; and *Z* direction was vertical direction. And this system was equipped with advanced integrated measure construction (IMC) data acquisition system, which could collect up to 144 accelerations and strain channel data.

Since gravity acceleration could not be changed, the similarity ratio of test acceleration was determined to be 1.0. Considering engineering practice and bearing capacity of shaking table, the geometric similarity ratio of tunnel lining and surrounding rock was 1/20, and the elastic modulus similarity ratio was 1/30. As shown in Table 1, other similar ratios were deduced by dimensional analysis method. According to the similarity ratio of lining thickness $C_h=C_l/C_E^{-1/3}$ [23], the similarity ratio of lining thickness was calculated as 1/6.44. The model fault dip was set as 90° in which prototype fault dip is nearly 90°. Figure 1 shows two-splicing mode of tunnels and faults location in model box.

The test model box was a welded steel model box with clearance sizes of 3.3 m×2.3 m×2.4 m (length×width×height). The box had a baseplate

Table 1 Similarity rules for shaking table tests

Parameter	Prototype	Similarity ratio	Model
Acceleration/*g*	0.20	C_A	0.20
Geometry/m	48.00	C_l	2.40
Elastic modulus/GPa	6.50	C_E	0.22
Density/(kg·m^{-3})	2.40	C_E/C_lC_A	1.92
Time/s	30.00	$\sqrt{C_l/C_A}$	7.19
Buried depth/m	40.00	C_l	2.00
Section height/m	9.59	C_l	0.48
Sectional area/m^2	60.99	C_l^2	0.15
Lining thickness/m	0.40	C_h	0.062
Fault thickness/m	7.00	C_l	0.35

Note: C_A−aueleration similarity ratio; C_l−geometry similarity ratio; C_E−elastic modulns similarity ratio; C_k−lining thichness similarity ratio.

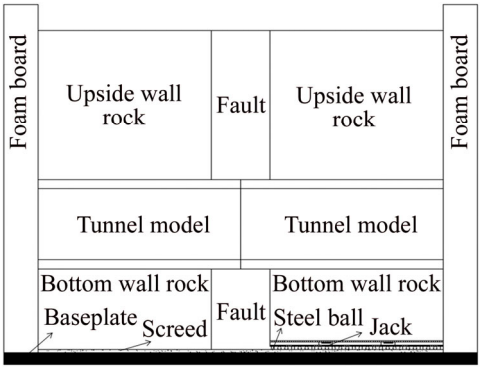

Figure 1 Arrangement of tunnel model in model box

with thickness of 15 mm, a 6 mm thick sidewall reinforced by No. 10 channel steel with a longitudinal and transverse spacing of 550 mm (as shown in Figure 2). To reduce the influence of rigid boundary of model box on test results, four inner walls of model box were paved with a polystyrene foam board with a thickness of 200 mm. A 50 mm thick mortar cushion was laid on the box baseplate to prevent a relative sliding between surrounding rock model and model box in test. Finally, the model box was fixed on the shaking table by ϕ20 bolts.

Figure 2 Model box

The tunnel lining and the surrounding rock were simulated by cement composited of quartz sand, barite powder, cement, gypsum and water [24, 25]. According to the mechanics performance of tunnel lining and surrounding rock and similarity ratio (Table 1), two mixture ratios of tunnel lining, strongly weathered rough rock and weakly rough rock for this test were determined, as shown in Table 2. Reinforcing bars in tunnel lining were simulated with fixed steel wire mesh with diameter of 0.6 mm and spacing of 12 mm [26]. And the fault of tunnel was simulated with gravel particle size of 10−20 mm.

Table 2 Proportion of similar materials (%)

Material	Quartz sand	Barite powder	Cement	Gypsum	Water
Tunnel lining	0.65	0.01	0.1	0.07	0.17
Strongly weathered rough rock	0.65	0.01	0.1	0.07	0.17
Weakly weathered rough rock	0.65	0.01	0.15	0.02	0.17

And a 1.2 m long wooden template of tunnel lining model was made, and the steel wire mesh was fixed in template. The template was poured by the mixture prepared in accordance with the above mixture ratios listed in Table 2, and was vibrated and compacted by a vibrator and thus two tunnel lining models were finished with a cure for 28 d and a dismantle after 7 d. Figure 3 shows the tunnel lining model after cure. Two kinds of surrounding rock simulation blocks (600 mm×900 mm×400 mm and 900 mm×900 mm×400 mm) were poured in line with the same procedure.

Figure 3 Tunnel lining model

In this experiment, a special sliding device of fault was designed and manufactured to realize three-dimensional fault sliding during experiment in Figure 4. A ball layer was arranged on the half of baseplate of model box; 12 rolling grooves with sizes of 100 mm×50 mm×2 mm (inner diameter× height×thickness) were arranged; 12 steel balls with a diameter of 40 mm were placed in the rolling grooves (Figure 4). Then a 10 mm thick steel plate with length of 1.8 m and width of 1.5 m was placed on the rigid ball, four 10 t synchronous hydraulic jacks (FPY-10, stroke 11 mm) were uniformly arranged on the steel plate, and another 10 mm thick steel plate was laid on the jacks to bear the weight of overlying surrounding rock. The sliding device of fault can realize vertical sliding of fault before seismic excitation and horizontal sliding during seismic excitation. Before seismic excitation, the jack in fault sliding device was started to drive the upper rock mass to rise, so as to realize fault vertical sliding. In the process of seismic excitation, the 12 steel balls fascinated the overlaying rock strata in model box to horizontally slip. In this experiment, we arranged acceleration sensors under

the bottom wall rock, and put them in the steel plate which were upward the jack (Figure 5). When we use the special sliding device of fault, the acceleration sensors will record the acceleration time curve during this period of time. Then we will calculate the displacement of the normal fault slip through the acceleration time curve by software. Through multiple experiments, we with finally achieve the normal fault slip magnitude ranging from 0 to 2 mm.

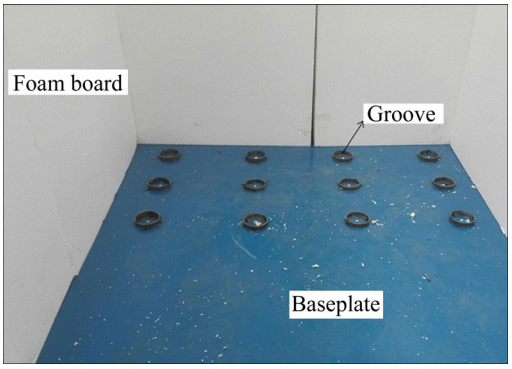

Figure 4 Normal fault slipping device

Figure 5 Acceleration sensors in steel plate

The fault sliding device was installed in model box. Then the surrounding rock model beneath tunnel, tunnel model, and the surrounding rock models at both sides of tunnel and top of tunnel were hoisted and installed into model box successively. Two tunnels with length of 1.2 m were bonded by epoxy resin adhesive and a layer of resin fiber cloth in model box. Surrounding rock materials with the same proportion were used to fill joints between layers and between surrounding rock blocks, so as to avoid a stratification of surrounding rock materials. A layer of plastic film was laid in fault fracture zone and surrounding rock to reduce the friction between them and further improve the fault sliding. After the completion of sample installation, the samples were rested for 10−13 h to realize a natural settlement [27−29].

2.3 Sensor arrangement

Figures 6 and 7 show the arrangement of acceleration sensors and strain gauge in this test. In Figure 6, the distribution of strain gauge on cross section of tunnel was marked from points A to N. Figure 7 shows the profile expansion of inner and outer wall of tunnel. The numbers of strain gages are S11−S16, S21−S26, S31−S36, S43−S46, S51−S56, S63−S66, S73−S76, S83−S86, S1(1)−S1(4), S2(1)−S2(4), S3(1)−S3(4), S4(1)−S4(4), S5(1)−S5(4), S6(1)−S6(4) along line from points A to N, respectively. The acceleration sensors were mainly arranged on a1, a2, a3. Because of the difficulty in arranging strain gages on Section 2 of tunnel inner wall, we didn't arrange any strain gages on these plates. So we didn't sign Section 2 in Figure 7(b).

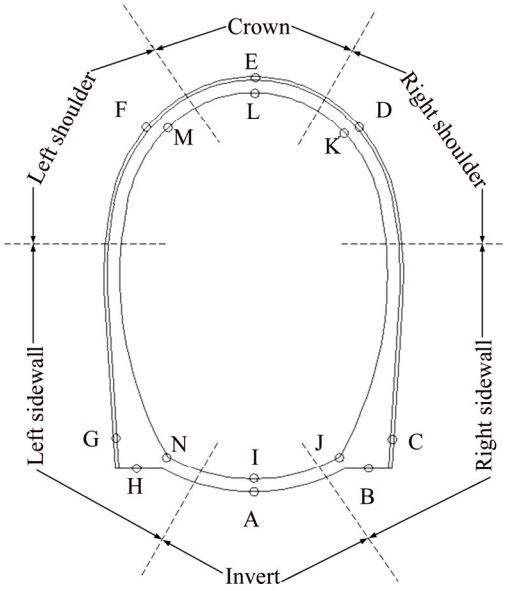

Figure 6 Arrangement of strain sensors

2.4 Seismic excitation input

In this test, El wave and Kobe wave were selected as input seismic excitation. El wave was recorded by El Centro Station during the 1940 Empire Valley earthquake in California, USA. Its original ground peak acceleration and fault distance were 0.28*g* and 6.1 km, respectively. Kobe wave was recorded in 2004 by Kobe University Station in

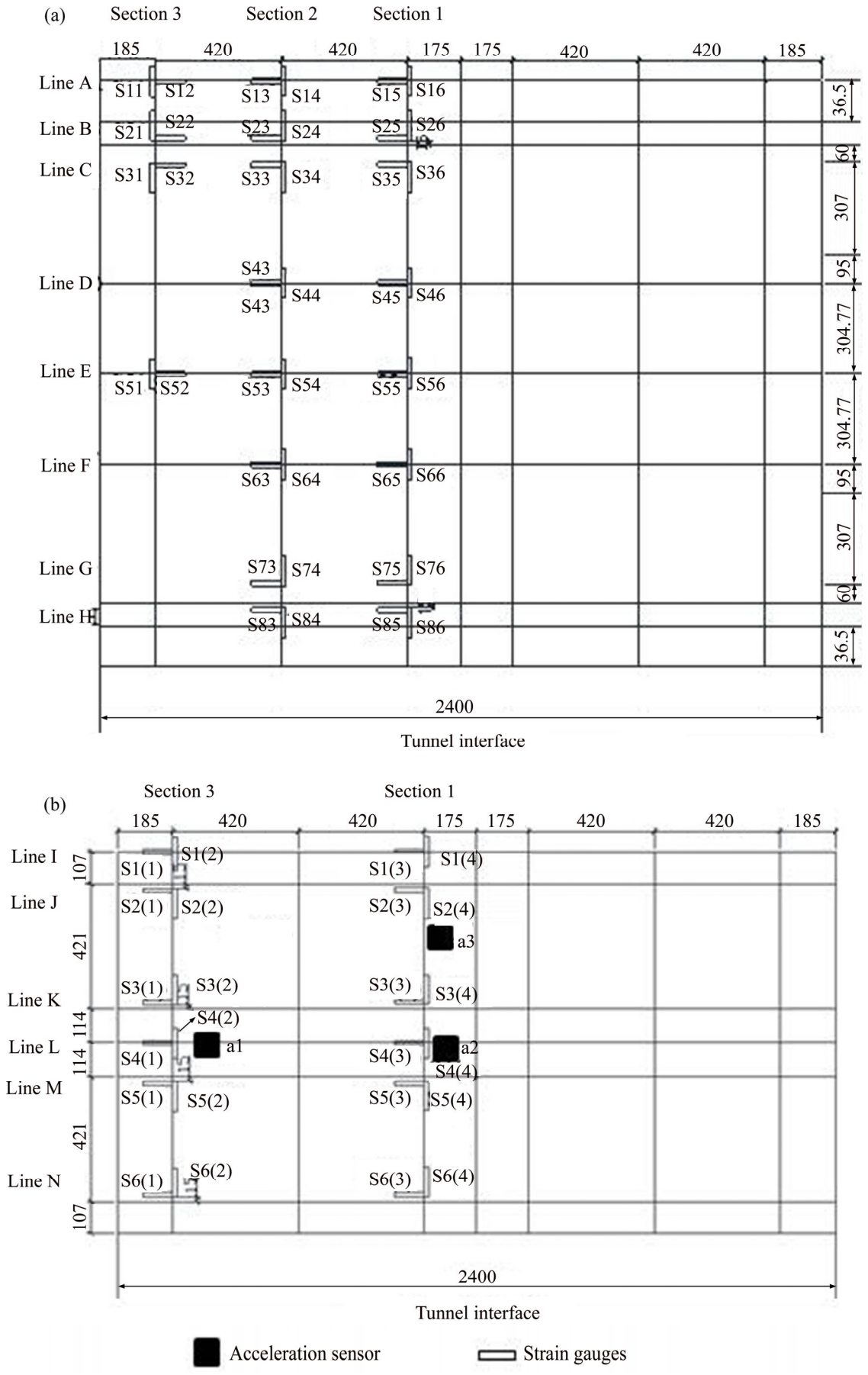

Figure 7 Arrangement of instrumentation (mm): (a) Tunnel outer wall; (b) Tunnel inner wall

Kobe, Japan. Its original peak ground acceleration and fault distance were 0.22*g* and 0.9 km, respectively. According to the time similarity ratio in Table 1, the time history curve of seismic wave was compressed, as shown in Figures 8(a) and (c); and the corresponding spectrum was obtained through Fourier transform, as shown in Figures 8(b) and (d). The frequency components of Kobe wave mainly ranged from 1.1 to 26.4 Hz and the dominant frequency was 2.6 Hz, while EI wave ranged from 2.0 to 41.2 Hz, and dominant one is 6.5 Hz. In Figure 8, the duration of compressed seismic wave is reduced from the similar ratio to about a quarter of original wave, so the main frequency is increased to about four times that of the original wave.

2.5 Test cases

21 test cases were designed for this test, as shown in Table 3. When 21 seismic excitations acted on a group of tunnel models in turn, a plastic deformation was probably accumulated in tunnel lining, which may affect the accuracy of test results. To reduce this adverse effect, fault sliding was applied in an ascending order in this test considering that only a group of tunnel models was used in this test. Before each case of experiment, the same white noise was used to detect the properties of tunnel model itself.

3 Results and discussion

3.1 Boundary effect

By comparing the acceleration peak at the same depth of tunnel model, the boundary effect of model box was evaluated. In this experiment, Eq. (1) was used to calculate Pearson product moment correlation coefficient [30].

$$r=\frac{\sum_{i=1}^{n}(a_i-\bar{a})(b_i-\bar{b})}{\sqrt{\sum_{i=1}^{n}(a_i-\bar{a})^2}\sqrt{\sum_{i=1}^{n}(b_i-\bar{b})^2}}=\frac{n\sum_{i=1}^{n}a_ib_i-\left(\sum_{i=1}^{n}a_i\right)\left(\sum_{i=1}^{n}b_i\right)}{\sqrt{n\sum_{i=1}^{n}a_i^2-\left(\sum_{i=1}^{n}a_i\right)^2}\sqrt{n\sum_{i=1}^{n}b_i^2-\left(\sum_{i=1}^{n}b_i\right)^2}} \quad (1)$$

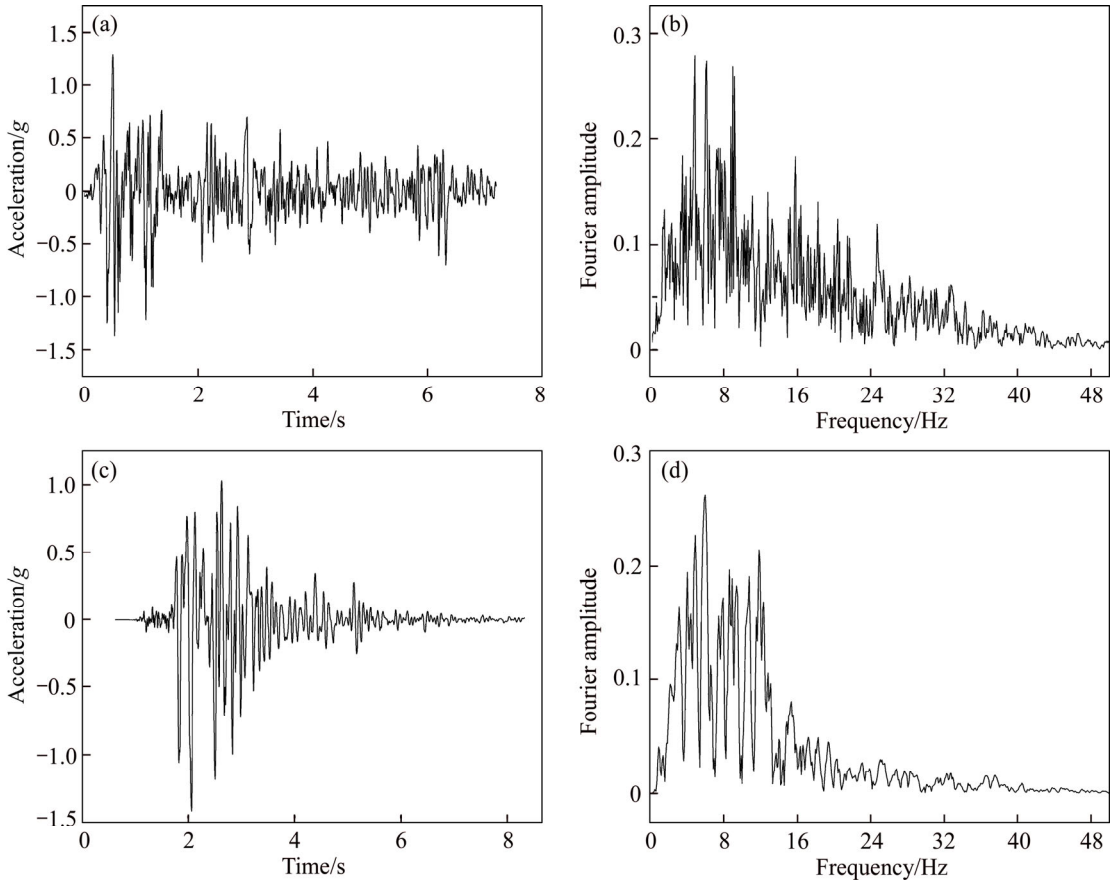

Figure 8 Acceleration−time histories and corresponding Fourier spectrum: (a) Acceleration−time histories of El wave; (b) Fourier spectrum of El wave; (c) Acceleration−time histories of Kobe wave; (d) Fourier spectrum of Kobe wave

Table 3 Loading sequence for shaking table tests

No.	Normal fault slip/mm	Input waveform		
		Name	PGA/*g*	Direction
1	0	WN	0.05	_
2	0	El	0.20	*x*
3	0	El	0.20	*y*
4	0	El	0.20	*z*
5	0	Kobe	0.20	*x*
6	0	Kobe	0.20	*y*
7	0	Kobe	0.20	*z*
8	1	WN	0.05	_
9	1	El	0.20	*x*
10	1	El	0.20	*y*
11	1	El	0.20	*z*
12	1	Kobe	0.20	*x*
13	1	Kobe	0.20	*y*
14	1	Kobe	0.20	*z*
15	2	WN	0.05	_
16	2	El	0.20	*x*
17	2	El	0.20	*y*
18	2	El	0.20	*z*
19	2	Kobe	0.20	*x*
20	2	Kobe	0.20	*y*
21	2	Kobe	0.20	*z*

Note: WN−white noise; PGA−peak ground acceleration.

where r is Pearson product moment correlation coefficient; a_i and b_i are the two acceleration values for comparison. Specifically, a_i (i=1, 2) represents the surrounding rock acceleration of position located in foam plate near the boundary end of tunnel axis and one near the boundary end of parallel tunnel axis, respectively; b_i (i=1, 2) represents the surrounding rock acceleration of tunnel at the same time as a_i (i=1, 2). Generally, if r≥0.9, the influence of boundary effect on results of model test can be ignored.

The acceleration measured at the above positions in test is substituted into Eq. (1) to obtain Pearson product moment correlation coefficient, as shown in Table 4. It can be seen that the influence of boundary effect of model box on test results can be ignored and the test results are reliable.

3.2 Acceleration response

Under the action of normal fault slip, the seismic acceleration of crown and sidewalls of tunnel in fault is shown in Figure 9. In Figure 9, *X*, *Y* and *Z* represent the *x*, *y* and *z* direction of acceleration under corresponding to *x*, *y* and *z* direction seismic excitation, respectively. As shown in Figure 9, the peak acceleration of *Z* direction on crown positioned at point S4(3) under *Z* direction seismic excitation is more than that under *X* or *Y* directions Kobe or El seismic excitation. And the peak of *Y* direction on the sidewall positioned at point S3(3) under *Y* direction seismic excitation is more than that under *X* or *Z* direction Kobe and El seismic excitation. Under 0.2*g* seismic excitation, the peak accelerations of tunnel in *X*, *Y* and *Z* directions under normal fault slip with 1 and 2 mm are closed to that with 0 mm, so the influence of small faults slip on seismic acceleration could be ignored. And the peak accelerations of tunnel generated by *X* direction seismic excitation are small.

Table 4 Acceleration correlation coefficient

Test ID	Boundary along tunnel axis	Boundary parallel tunnel axis
El	0.967	0.959
Kobe	0.968	0.932

3.3 Strain response

The incremental strain response of tunnel generated by *X* direction seismic excitation is small. Therefore, the tunnel incremental strain responses generated by *Y* and *Z* directions seismic excitation are merely discussed in this section.

Figure 10 shows the incremental strain of outer tunnel lining in fault under fault sliding and seismic excitation of El wave. Figures 10 (a) and (b) show that under *Y* direction of seismic excitation, the incremental strains on outer wall of sidewall points B and C are the largest among points A to H in Figure 6. Figures 10(c) and (d) show that under *Z* direction of seismic excitation, the incremental strain on outer wall of inverting point A is larger than those on other points plotted in Figure 6. Figure 10(b) shows that when fault vertical slip increases from 0 to 2 mm, the maximum incremental strain of the outer tunnel lining in fault obviously increases from 40με to 100με. And this might induce tunnel lining to fracture. So, it could deduce that fault vertical slip increases the incremental seismic strain response of tunnel lining, and the tunnel lining is more valuable damage undergoing normal fault slip and

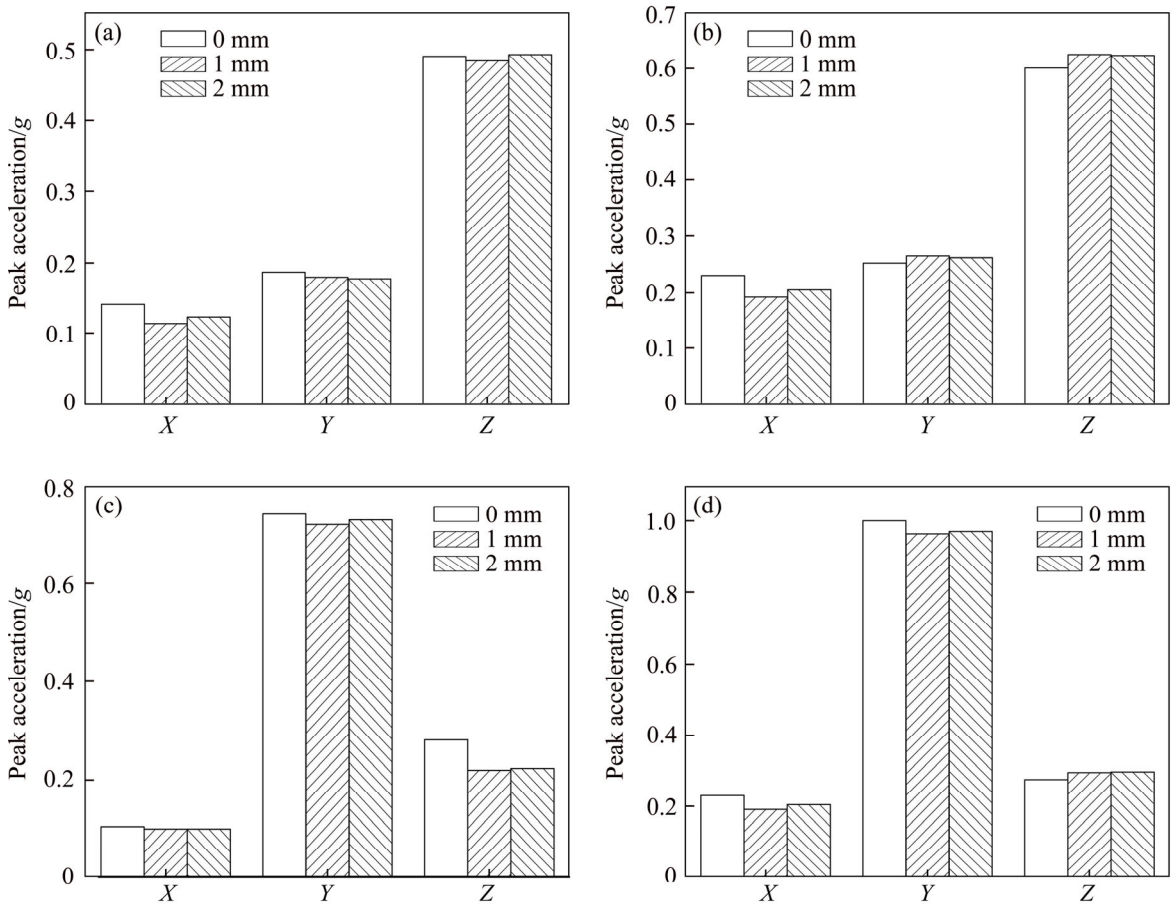

Figure 9 Variation of peak acceleration with normal fault slips: (a) Kobe wave tunnel crown; (b) El wave tunnel crown; (c) Kobe wave tunnel sidewall; (d) El wave tunnel sidewall in fault

earthquake than only undergoing earthquake.

Figure 11 shows the incremental strain of outer sidewall of tunnel under fault sliding and *Y* direction seismic excitation. Figures 11 (a) and (b) show that under El and Kobe wave excitation, the incremental strain on outer wall of sidewall along line C (shown in Figure 7) decreased with increasing of distance from the fault among 0 (point S36 in Section 1), 420 (point S34 in Section 2) and 840 mm (point S31 in Section 3) under the fault sliding of 0, 1 and 2 mm, respectively. And the change of incremental strain along line B for point S26 in Section 1, S24 in Section 2, and S21 in Section 3 is the same to that along line C.

Figure 11(a) also shows that the incremental strains of outer wall of sidewall on Section 1 (0 mm) and Section 2 (420 mm, 1.2 times fault thickness) increase under *Y* direction excitation when the normal fault slip increases from 0 to 2 mm. This suggests that normal fault slip could amplify the strains of outer sidewall zone with 1.7 times fault thickness and centered in tunnel fault under 0.2*g* seismic excitation. The reason is speculated that the outer wall of concrete tunnel lining is subjected to tension deformation caused by normal fault slip before seismic excitation, and a more incremental strain is generated by a seismic excitation. So, the incremental strain induced by normal slip or seismic excitation is larger than that only induced by seismic excitation. The incremental strain response on sidewall of tunnel lining in fault is similar.

Figure 12 shows the incremental strain of outer wall of crown under fault sliding and *Z* direction seismic excitation. Figure 12 shows that under El and Kobe wave excitation, the incremental strain on outer wall of crown along line E decreases with increasing of distance from the fault between 0 (point S56 in Section 1) and 840 mm (point S51 in Section 3) under the fault sliding of 0, 1 and 2 mm, respectively. And the change of incremental strain of invert along line A on point S16 in Section 1 or S11 in Section 3 is the same to that along line C.

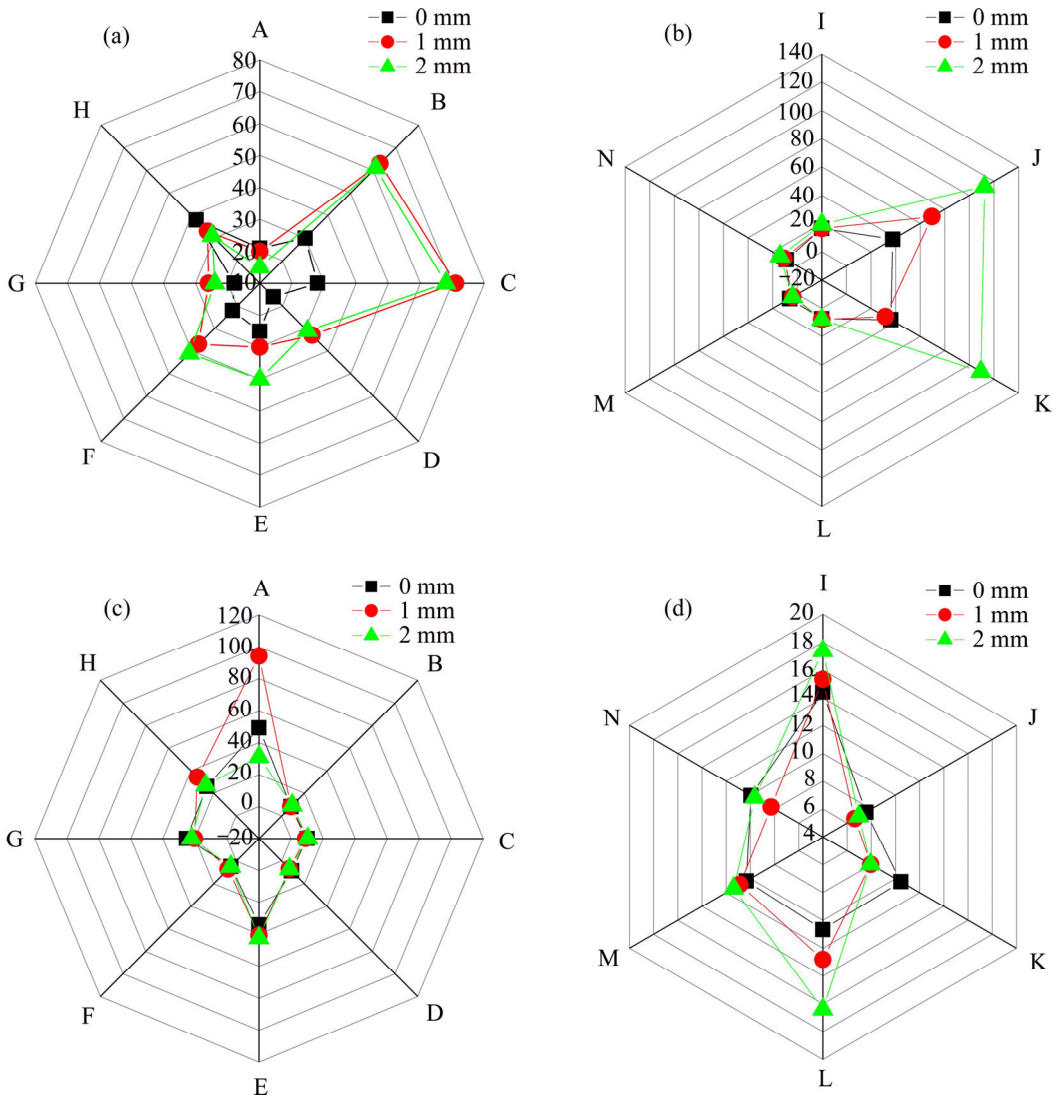

Figure 10 Incremental strain of tunnel lining in fault induced by El wave (unit: με): (a) On outer wall under *Y* direction; (b) On inner wall under *Y* direction; (c) On outer wall under *Z*-direction; (d) On inner wall under *Z* direction

As shown in Figure 12, faults slips have a significant amplification effect on the incremental strain response of tunnel lining, and little effect on the tunnel lining zone far away fault with distance of 2.4 times thickness. At the same time, with the increase of normal fault slip, the overall incremental strain of outer wall of tunnel in fault shows an upward trend. Besides, there is a large incremental strain on tunnel invert inducing a tensile action and small incremental strain on crown in which the *Z* direction seismic excitation is the same to the direction of normal fault slip. Thus, it is inferred that the increase of incremental seismic strain on crown and invert is caused by normal fault slip.

Figures 13 and 14 show the incremental seismic strain of inner wall of tunnel crown in fault under normal fault slip. Figures 13 and 14 show that under El and Kobe wave excitation, the incremental strain on outer wall of sidewall along line L decreases with the increase of distance from the fault between 0 (point S4(4) in Section 1) and 840 mm (point S4(1) in Section 3) under the fault sliding of 0, 1 and 2 mm, respectively. And the change of incremental strain along line I on point S1(4) in Section 1, S1(2) in Section 3 is the same to that along line L.

It could be seen from Figures 11 and 13 that under the normal fault slip of 0−2 mm, the incremental strain of inner wall was smaller than that of outer wall at the same position of tunnel. However, under normal fault slip of 2 mm, the incremental seismic strain of inner wall of crown and invert in fault exceeds 100με. And it could be suggested that a large normal fault slip has a great

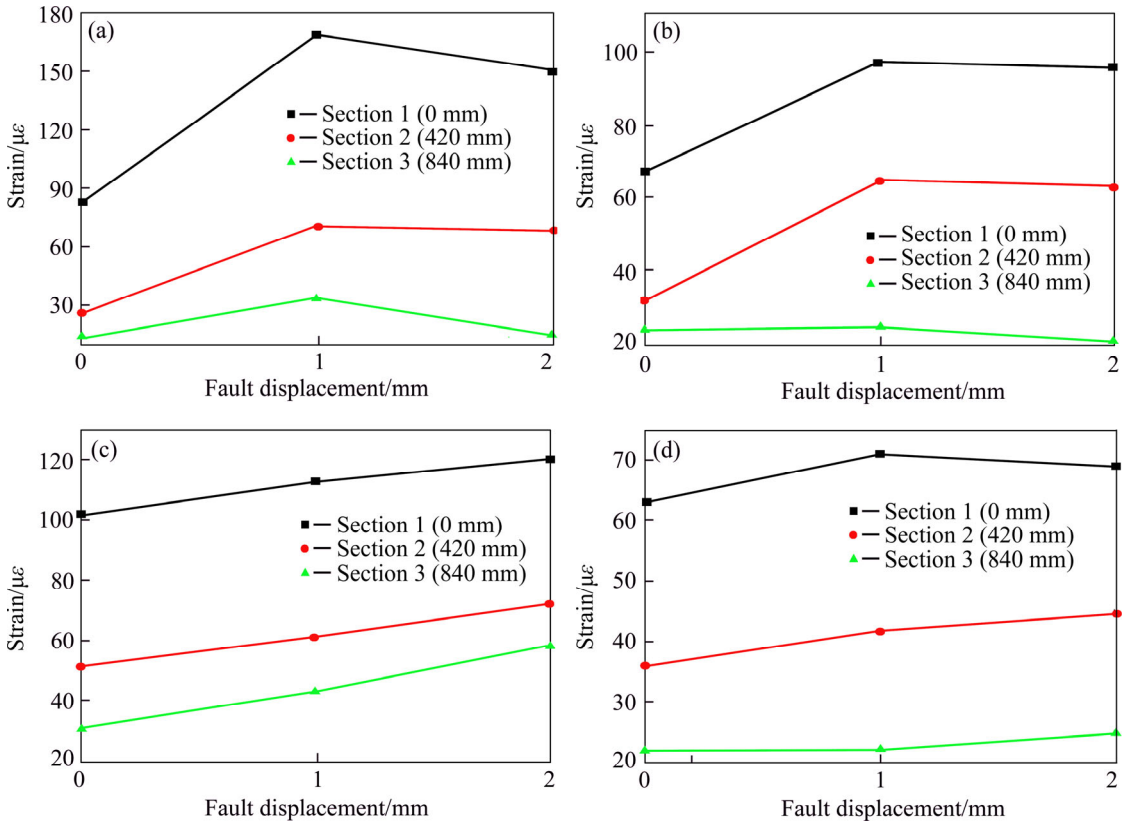

Figure 11 Outer sidewall incremental strain in *Y* direction seismic excitation: (a) Along line C excited by Ei wave; (b) Along line B excited by Ei wave; (c) Along line C excited by Kobe wave; (d) Along line B excited by Kobe wave

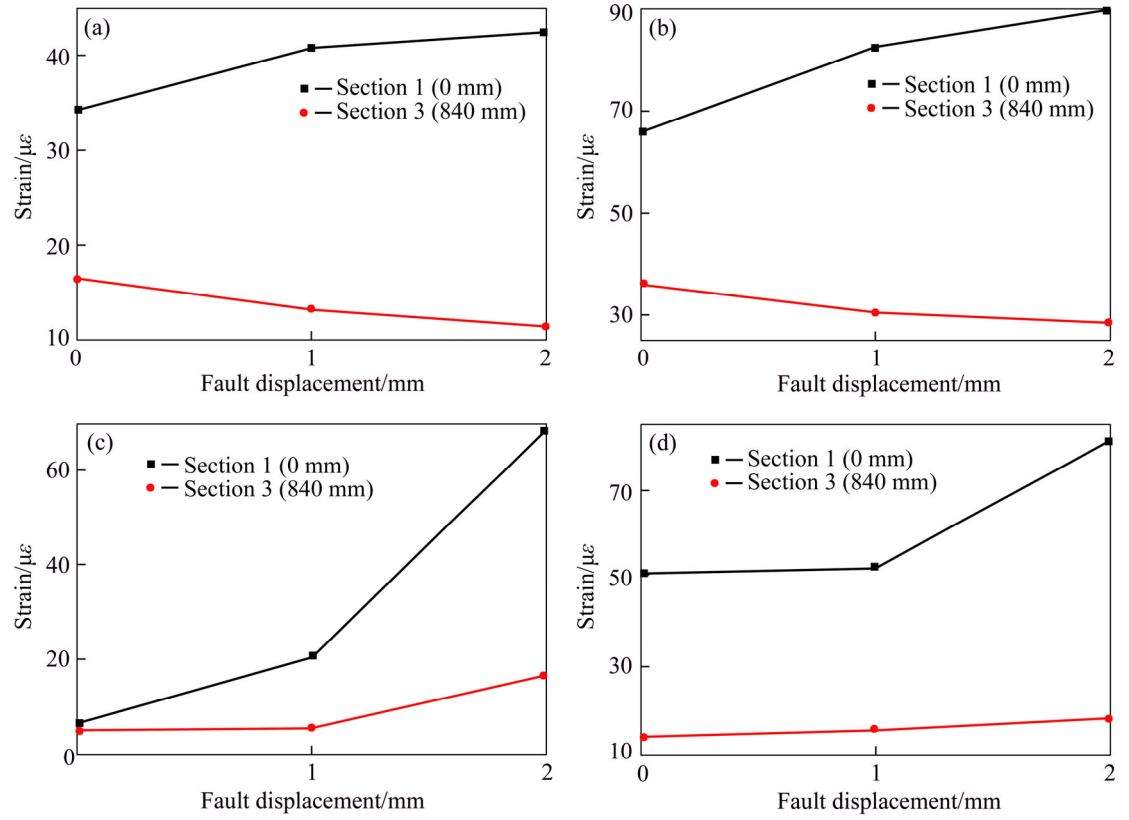

Figure 12 Outer wall incremental strain in *Z* direction seismic excitation: (a) Crown strain under El wave excitation; (b) Invert strain under El wave excitation; (c) Crown strain under Kobe wave excitation; (d) Invert strain under Kobe wave excitation

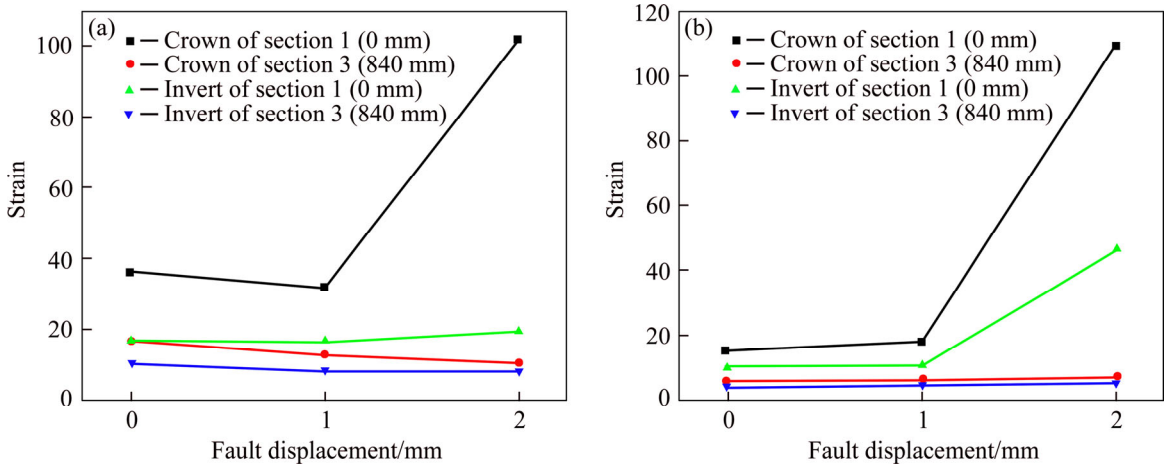

Figure 13 Incremental strain on inner wall in *Z* direction seismic excitation: (a) El wave; (b) Kobe wave

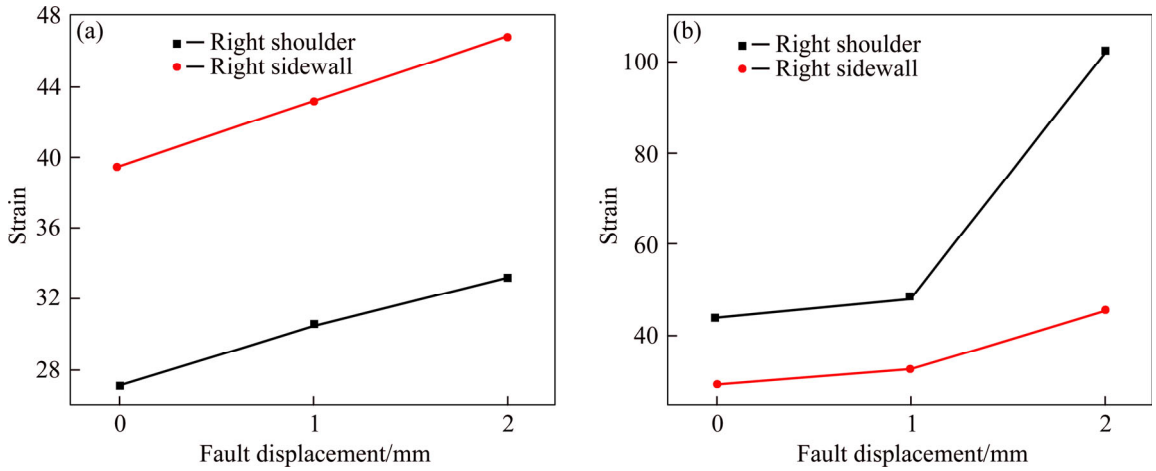

Figure 14 Incremental strain on inner wall of tunnel in *Y* direction excitation: (a) El wave; (b) Kobe wave

impact on the seismic strains of tunnel inner wall. It can also be seen from Figure 14 that under fault slip and *Y* direction seismic excitation, the incremental strain of the inner wall of sidewall is larger than that of shoulder.

A numerical simulation result of tunnel crossing fault shows that under the action of normal fault slip, the sidewall is most affected, while the crown and invert are least affected [31−33]. While under the joint action of normal fault slip and 0.2*g* seismic excitation, the right sidewall of lining in fault is mainly affected by *Y* direction seismic excitation; the crown and invert of lining in fault is mainly affected by *Z* direction seismic excitation.

3.4 Influence of normal fault slip on characteristic frequency of tunnel model

Referring to the tunnel lining damage identification technology [34], the accelerations of crown and sidewall of tunnel in fault layer collected from the white noise in cases 1, 8 and 15 are Fourier transformed to obtain the frequency spectrum of each working condition. The characteristic frequencies of tunnel model in cases 1, 8 and 15 are obtained, as shown in Figure 15. It could be seen from Figure 15 that the characteristic frequency of tunnel model is reduced from 21.85 to

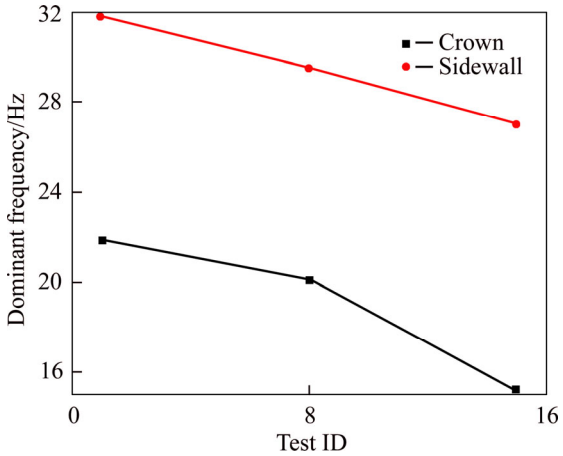

Figure 15 Variation of dominant frequencies with seismic excitation and normal fault slip

15.15 Hz, and that of the sidewall is reduced from 31.8 to 27.04 Hz. Therefore, the characteristic frequency of tunnel decreases with increase of normal fault slip. It indicates that the overall stiffness of tunnel decreases obviously under the action of normal fault slip and earthquake.

4 Conclusions

In this experiment, a new type of fault sliding device is designed, and the seismic response of tunnel across a fault under the normal fault slip is studied by shaking table tests. The main conclusions are drawn as follows:

1) Peak acceleration of lining is dominated by the existence of fault and direction of seismic excitation, not normal fault slip.

2) Incremental strains of lining in critical zone with 1.7 times fault thickness and centered in faults induced by normal fault slip and seismic excitation are larger than that only by seismic excitation. And the incremental strains in critical zone increase with increases of normal fault slip magnitude ranging from 0 to 2 mm.

3) Under action of normal fault slip, the sidewall and invert have a maximum incremental strain under *Y* and *Z* direction seismic excitation, respectively.

4) Normal fault slip results in a significant reduction of overall tunnel stiffness after earthquake excitation.

References

[1] WANG Zheng-zheng, ZHANG Zhe. Seismic damage classification and risk assessment of mountain tunnels with a validation for the 2008 Wenchuan earthquake [J]. Soil Dynamics and Earthquake Engineering, 2013, 45(2): 45−55. DOI: 10.1016/ j.soildyn.2012.11.002.

[2] YU Hai-tao, CHEN Jun-tao, BOBET A, YUAN Yong. Damage observation and assessment of the Longxi tunnel during the Wenchuan earthquake [J]. Tunnelling and Underground Space Technology, 2016, 54: 102−116. DOI: 10.1016/j.tust.2016.02.008.

[3] SHEN Yu-sheng, GAO Bo, YANG Xiao-ming, TAO Shuang-jiang. Seismic damage mechanism and dynamic deformation characteristic analysis of mountain tunnel after Wenchuan earthquake [J]. Engineering Geology, 2014, 180: 85−98. DOI: 10.1016/j.enggeo.2014.07.017.

[4] LI Tian-bin. Damage to mountain tunnels related to the Wenchuan earthquake and some suggestions for aseismic tunnel construction [J]. Bulletin of Engineering Geology and the Environment, 2012, 71(2): 297−308. DOI: 10.1007/ s10064-011-0367-6.

[5] WANG W L, WANG T T, SU J J, LIN C H, SENG C R, HUANG T H. Assessment of damage in mountain tunnels due to the Taiwan Chi-Chi earthquake [J]. Tunnelling and Underground Space Technology, 2001, 16: 133−150. DOI: 10.1016/S0886-7798(01)00047-5.

[6] HASHASH Y M, HOOK J J, SCHMIDT B, YAO I C. Seismic design and analysis of underground structures [J]. Tunnelling and Underground Space Technology, 2001, 16: 247−293. DOI: 10.1016/S0886-7798(01)00051-7.

[7] KIANI M, AKHLAGHI T, GHALANDARZADEH A. Experimental modeling of segmental shallow tunnels in alluvial affected by normal faults [J]. Tunnelling and Underground Space Technology, 2016, 51: 108−119. DOI: 10.1016/j.tust.2015.10.005.

[8] KIANI M, GHALANDARZADEH A, AKHLAGHI T, AHMADI M. Experimental evaluation of vulnerability for urban segmental tunnels subjected to normal surface faulting [J]. Soil Dynamics and Earthquake Engineering, 2016, 89: 28−37. DOI: 10.1016/j.soildyn.2016.07.012.

[9] MA Y, SHENG Qian, ZHANG Gui-min, CUI Zhen. A 3D discrete-continuum coupling approach for investigating the deformation and failure mechanism of tunnels across an active fault: A case study of Xianglushan tunnel [J]. Applied Sciences, 2019, 8(9): 11−25. DOI: 10.3390/ app9112318.

[10] LIU Xue-zeng, LI Xue-feng, SANG Yun-long, LIN Liang-lun. Experimental study on normal fault rupture propagation in loose strata and its impact on mountain tunnels [J]. Tunnelling and Underground Space Technology, 2015, 49: 417−425. DOI: 10.1016/j.tust.2015.05.010.

[11] ZHANG Zhi-qiang, CHEN Fang-fang, LI Ning, SWOBODA G, LIU Nai-fei. Influence of fault on the surrounding rock stability of a tunnel: Location and thickness [J]. Tunnelling and Underground Space Technology, 2017, 61: 1−11. DOI: 10.1016/j.tust.2016.09.003.

[12] KUN M, ONARGAN T. Influence of the fault zone in shallow tunneling: A case study of Izmir Metro Tunnel [J]. Tunnelling and Underground Space Technology, 2013, 33: 34−45. DOI: 10.1016/j.tust.2012.06.016.

[13] XIN Chun-lei, GAO Bo, WEN Gao-ming, ZHOU Jia-mei, SHEN Yu-sheng, QUAN Xiao-juan. Study on seismic failure characteristics and anti-shock reduction measures of straddle-slip fault tunnel [J]. Journal of Vibration Engineering, 2016, 29(4): 694−703. DOI: 10.16385/j.cnki. issn.1004-4523.2016.04.017. (in Chinese)

[14] XIN Chun-lei, GAO Bo, WANG Ying-xue, ZHOU Jia-mei, SHEN Yu-sheng. Shaking table test on deformable aseismic and damping measures for fault-crossing tunnel structures [J]. Rock and Soil Mechanics, 2015, 36(4): 1041−1049. DOI: 10.16285/j.rsm.2015.04.019. (in Chinese)

[15] XIN Chun-lei, GAO Bo, ZHOU Jia-mei. SHEN Yu-sheng, QUAN Xiao-juan. Shaking table tests on performances of anti-seismic and damping measures for fault-crossing tunnel structures [J]. Chinese Journal of Geotechnical Engineering, 2014, 36(8): 1414−1422. DOI: 10.11779/CJGE201408006.

(in Chinese)

[16] YAN Gao-ming, GAO Bo, SHENG Yu-sheng, ZHENG Qing, FAN Kai-xiang, HUANG Hai-feng. Shaking table test on seismic performances of newly designed joints for mountain tunnels crossing faults [J]. Advances in Structural Engineering, 2020, 23(2): 248−262. DOI: 10.1177/1369433219868932.

[17] MA Ju, DONG Long-jun, ZHAO Guo-yan, LI Xi-bing. Qualitative method and case study for ground vibration of tunnels induced by fault-slip in underground mine [J]. Rock Mechanics and Rock Engineering, 2019, 52: 1887−1901. DOI: 10.1007/s00603-018-1631-x.

[18] ANASTASOPOULOS L, GEROLYMOS N, DROSOS V,GEORGARAKOS T, KOURKOULIS R, GAZETAS G. Behaviour of deep immersed tunnel under combined normal fault rupture deformation and subsequent seismic shaking [J]. Bulletin of Earthquake Engineering, 2008, 9(6): 213−239. DOI: 10.1007/s10518-007-9055-0.

[19] FANG Lin, JIANG Shu-ping, LIN Zhi, WANG Fang-qi. Shaking table model test study of tunnel through fault [J]. Rock and Soil Mechanics, 2011, 32(9): 2709−2820. DOI: 10.1111/j.1759-6831.2010.00113.x. (in Chinese)

[20] LIU Li-biao, WANG Yong-fu, LIU Fang, ZHOU Jie. Shaking table model tests on the influence of fault strike on the seismic responses of tunnels [J]. Journal of Vibration and Shock, 2017, 36(21): 196−201. DOI: 10.13465/j.cnki.jvs.2017.21.029. (in Chinese)

[21] BAKER B H, WOHLENBERG J. Structure and evolution of the kenya rift valley [J]. Nature, 1971, 229(5286): 538−542. DOI: 10.1038/229538a0.

[22] MACDONALD R. Petrological evidence regarding the evolution of the kenya rift valley [J]. Tectonophysics, 1994, 236(1−4): 373−390. DOI: 10.1016/0040-1951(94)90185-6.

[23] LAI Hong-peng, XIE Yong-li, YANG Xiao-hua. Model test study on section form of highway tunnel lining [J]. Chinese Journal of Geotechnical Engineering, 2006, 63(28): 740−744. DOI: 10.3321/j.issn:1000-4548.2006.06.012. (in Chinese)

[24] PENG Shu-quan, WANG Fan, LI Xi-bing, FAN Ling, GONG Feng-qiang. A microbial method for improving salt swelling behavior of sulfate saline soil by an experimental study [J]. Alexandria Engineering Journal, 2019, 58: 1353−1366. DOI: 10.1016/j.aej.2019.11.006.

[25] PENG Shu-quan, WANG Fan, LI Xi-bing, FAN Ling. Experimental research on employed expanded polystyrene (EPS) for lightened sulfate heave of subgrade by thermal insulation properties [J]. Geotextiles and Geomembranes, 2020, 2: 9−18. DOI: 10.1016/j.geotexmem.2020.02.009.

[26] LI Yu-shu, LI Tian-bin, WANG Dong, XU Hua, LIU Ji. Large-scale shaking table model test for vibration-absorption measures of portal section Huangcaoping tunnel No. 2 [J]. Journal of Rock Mechanics and Engineering, 2009, 28(6): 1128−1136. DOI: 10.3321/j.issn:1000-6915.2009.06.006. (in Chinese)

[27] GUAN Zhen-chang, ZHOU Yi, GOU Xiao-dong, HUANG Hong-wei, WU Xue-zhen. The seismic responses and seismic properties of large section mountain tunnel based on shaking table tests [J]. Tunnelling and Underground Space Technology, 2019, 90: 383−393. DOI: 10.1016/j.tust.2019.05.017.

[28] CHEN Jian-yun, LI Jing, SUN Sheng-nan, SU Zhi-bin. Experimental and numerical analysis of submerged floating tunnel [J]. Journal of Central South University, 2012, 19: 2949−2957. DOI: 10.1007/s11771-012-1363-0.

[29] CHEN Qing-jun, YUAN Wei-ze, LI Ying-cheng, CAO Li-ya. Dynamic response characteristics of super high-rise buildings subjected to long-period ground motions [J]. Journal of Central South University, 2013, 30: 1341−1353. DOI: 10.1007/s11771-013-1621-9.

[30] XIN Chun-lei, WANG Zheng-zheng, GAO Bo. Shaking table tests on seismic response and damage mode of tunnel linings in diverse tunnel-void interaction states [J]. Tunnelling and Underground Space Technology, 2018, 77: 295−304. DOI: 10.1016/j.tust.2018.03.010.

[31] SHAO Run-meng, ZHAO Bo-ming. Longitudinal seismic response of large sectional shield tunnel [C]// Advances in Environmeatal Vibration. Beijing: Science Press, 2011: 313−319.

[32] LIU Ke-wei, LI Xu-dong, HAO Hong, LI Xi-bing, SHA Yan-yan, WANG Wei-hua, LIU Xi-ling. Study on the raising technique using one blast based on the combination of long-hole presplitting and vertical crater retreat multiple-deck shots [J]. International Journal of Rock Mechanics and Mining Sciences, 2019, 113: 41−58. DOI: 10.1016/j.ijrmms.2018.11.012.

[33] LIU Ke-wei, YANG Jia-cai, LI Xi-bing, HAO Hong, LI Qi-yue, LIU Zhi-xiang, WANG Chun-yi. Study on the long-hole raising technique using one blast based on vertical crater retreat multiple deck shots [J]. International Journal of Rock Mechanics and Mining Sciences, 2018, 109: 52−67. DOI: 10.1016/j.ijrmms.2018.06.020.

[34] XIN Chun-lei, WANG Zheng-zheng, ZHOU Jia-mei, GAO Bo. Shaking table tests on seismic behavior of polypropylene fiber reinforced concrete tunnel lining [J]. Tunnelling and Underground Space Technology, 2019, 88: 1−15. DOI: 10.1016/j.tust.2019.02.019.

(Edited by ZHENG Yu-tong)

中文导读

跨活断层隧道地震响应模型试验

摘要：穿越地震活跃带内的滑动活断层山岭隧道，极易受到活断层滑动和地震作用。研究断层滑动和地震作用下隧道动力学响应很有必要。本文设计了三维活断层滑动装置，通过振动台模型试验研究了活断层滑动作用下隧道地震性能。结果表明，在断层滑动和地震共同作用下，水平垂直隧道轴线地震波引起隧道衬砌侧壁产生较大响应，竖直方向地震波引起隧道衬砌拱顶产生较大响应，隧道衬砌加速度响应值受断层滑动量影响较小。水平垂直隧道轴线地震波引起的隧道断层段衬砌侧壁受拉应变较大，且随着断层滑移量的增加而增加，其他位置拉应变较小。竖直方向地震波引起的隧道断层段衬砌拱顶和拱底外壁受拉应变较大，且随着断层滑移量的增加而增加，其他位置拉应变较小。断层滑动对隧道整体刚度产生一定程度的影响，使隧道的整体刚度在地震激励作用后，出现明显的降低。本文结果可为隧道震害的防治措施及抗减震设计提供参考。

关键词：隧道；正断层；地震；断层滑动；振动台试验；峰值加速度